New giant carnivorous dinosaur reveals convergent evolutionary trends in theropod arm reduction

Highlights

- Meraxes, a new, giant predatory dinosaur from Patagonia had short arms like T. rex
- Meraxes is the most complete carcharodontosaurid yet from the Southern Hemisphere
- It documents peak diversity of carcharodontosaurids just before they went extinct
- Meraxes documents convergent evolution of short arms among megapredatory theropods.

Authors

Juan I. Canale, Sebastián Apesteguía, Pablo A. Gallina, ..., Alejandro Haluza, Federico A. Gianechini, Peter J. Makovicky

Correspondence

jicanale@unrn.edu.ar

In brief

Canale et al. describe a new species of carcharodontosaurid, *Meraxes gigas*, from Patagonia. *Meraxes* adds evidence for a peak in carcharodontosaurid diversity just before their extinction in the Late Cretaceous. With short forelimbs like *T. rex*, *Meraxes* documents convergent evolution of this trait among large, predatory theropod lineages.





Report

New giant carnivorous dinosaur reveals convergent evolutionary trends in theropod arm reduction

Juan I. Canale, 1,2,3,11,* Sebastián Apesteguía, 1,4 Pablo A. Gallina, 1,4 Jonathan Mitchell, 5 Nathan D. Smith, 6 Thomas M. Cullen, 7,8 Akiko Shinya,8 Alejandro Haluza,2 Federico A. Gianechini, 1,9 and Peter J. Makovicky 8,10 ¹CONICET, Buenos Aires, Argentina

9 Instituto Multidisciplinario de Investigaciones Biológicas de San Luis (IMIBIO-SL), CONICET-Universidad Nacional de San Luis. Área de Zoología, Facultad de Química, Bioquímica y Farmacia, UNSL. Ejército de los Andes 950, 5700 San Luis, Argentina

SUMMARY

Giant carnivorous dinosaurs such as Tyrannosaurus rex and abelisaurids are characterized by highly reduced forelimbs that stand in contrast to their huge dimensions, massive skulls, and obligate bipedalism. 1,2 Another group that follows this pattern, yet is still poorly known, is the Carcharodontosauridae: dominant predators that inhabited most continents during the Early Cretaceous³⁻⁵ and reached their largest sizes in Aptian-Cenomanian times. 6-10 Despite many discoveries over the last three decades, aspects of their anatomy, especially with regard to the skull, forearm, and feet, remain poorly known. Here we report a new carcharodontosaurid, Meraxes gigas, gen. et sp. nov., based on a specimen recovered from the Upper Cretaceous Huincul Formation of northern Patagonia, Argentina. Phylogenetic analysis places Meraxes among derived Carcharodontosauridae, in a clade with other massive South American species. Meraxes preserves novel anatomical information for derived carcharodontosaurids, including an almost complete forelimb that provides evidence for convergent allometric trends in forelimb reduction among three lineages of large-bodied, megapredatory non-avian theropods, including a remarkable degree of parallelism between the latestdiverging tyrannosaurids and carcharodontosaurids. This trend, coupled with a likely lower bound on forelimb reduction, hypothesized to be about 0.4 forelimb/femur length, combined to produce this short-armed pattern in theropods. The almost complete cranium of *Meraxes* permits new estimates of skull length in Giganotosaurus, which is among the longest for theropods. Meraxes also provides further evidence that carchardontosaurids reached peak diversity shortly before their extinction with high rates of trait evolution in facial ornamentation possibly linked to a social signaling role.

RESULTS

Systematic paleontology

Theropoda Marsh, 1881. Tetanurae Gauthier, 1986. Allosauroidea Marsh, 1878. Carcharodontosauridae Stromer, 1931. Carcharodontosaurinae Stromer, 1931. Giganotosaurini Coria and Currie, 2006. Meraxes gigas gen. et sp. nov.

Etymology

Meraxes after a dragon of the Song of Ice and Fire fiction series by George R.R. Martin. And gigas (Greek: giant) referring to the enormous size of the species.

Holotype

MMCh-PV 65 (Museo Municipal "Ernesto Bachmann," Villa El Chocón, Neuguén, Argentina), nearly complete skull without mandibles, pectoral and pelvic girdles, fore- and hindlimbs, fragments of cervical and dorsal vertebrae, complete sacrum, and proximal and middle caudal vertebral series (Figures 1, 2, and S1).

²Área Laboratorio e Investigación, Museo Municipal "Ernesto Bachmann," Villa El Chocón 8311, Neuquén, Argentina

³Universidad Nacional de Río Negro (UNRN), Isidro Lobo 516, R8332 Gral. Roca, Río Negro, Argentina

⁴Área de Paleontología, Fundación de Historia Natural Félix de Azara, CCNAA, Universidad Maimónides, Hidalgo 775, 1405 Ciudad Autónoma de Buenos Aires, Argentina

⁵West Virginia University Institute of Technology, 410 Neville Street, Life Sciences 119, Beckley, WV 25801 USA

⁶Dinosaur Institute, Natural History Museum of Los Angeles County, 900 Exposition Boulevard, Los Angeles, CA 90007 USA

⁷Ottawa-Carleton Geoscience Centre, Department of Earth Sciences, Carleton University, 1125 Colonel By Drive, Ottawa, ON K1S 5B6,

⁸ Negaunee Integrative Research Center, The Field Museum of Natural History, 1400 S. DuSable Lake Shore Drive, Chicago, IL 60605,

¹⁰Department of Earth and Environmental Sciences, University of Minnesota – Twin Cities, 116 Church Street SE, Minneapolis, MN 55455 USA ¹¹Lead contact

^{*}Correspondence: jicanale@unrn.edu.ar https://doi.org/10.1016/j.cub.2022.05.057



Current Biology Report

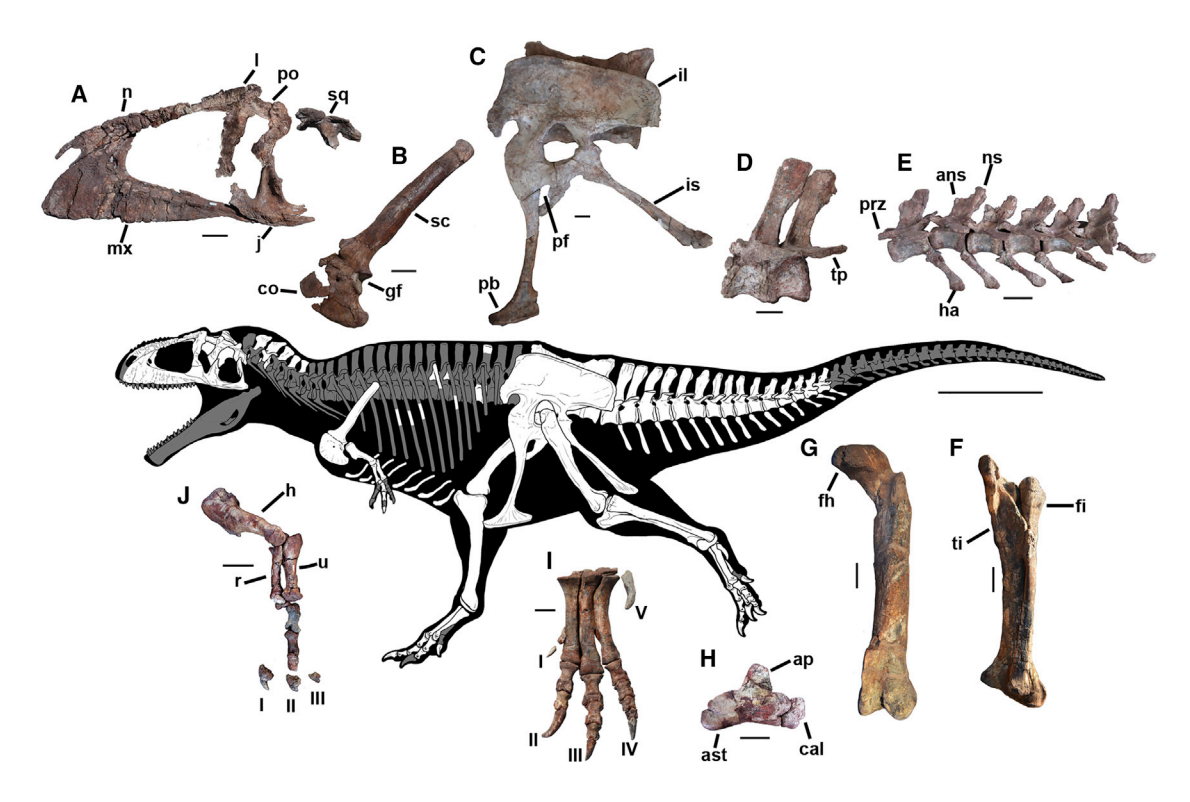


Figure 1. Meraxes gigas MMCh-PV 65

Reconstruction of the skeleton showing recovered bones in white.

- (A) Left side of the skull.
- (B) Right scapulocoracoid (reversed).
- (C) Right complete pelvis (reversed).
- (D) First two caudal vertebrae.
- (E) Articulated 10th to 15th caudal vertebrae series (reversed).
- (F) Left articulated tibia and fibula in anterolateral view.
- (G) Left femur in anterior view.
- (H) Left astragalus and calcaneum articulated in anterior view.
- (I) Left foot in anterior/dorsal view.
- (J) Articulated right arm (reversed) in lateral view (note that the unguals are shown in side view, instead of their articulated position).

ans, accessory neural spine; ast, astragalus; ap, ascending process; cal, calcaneum; co, coracoid; fh, femoral head; fi, fibula; qf, glenoid fossa; h, humerus; ha, hemal arch; il, ilium; is, ischium; j, jugal; I, lacrimal; mx, maxilla; n, nasal; ns, neural spine; pb, pubic boot; pf, pubic foramen; po, postorbital; prz, prezygapophysis; r, radius; sc, scapula; sq, squamosal; ti, tibia; tp, transverse process; u, ulna.

Individual scale bars, 10 cm; general scale bar, 1 m. Skeletal drawing made by Jorge A. Gonzalez. See also Figures S1 and S2 and Tables S1-S3.

Locality and horizon

Huincul Formation, 13 m above the conformable contact with the underlying Candeleros Formation (late Cenomanian-Turonian), of the Neuquén Group, 11 in Las Campanas Canyon, 25 km southwest of Villa El Chocón, Neuquén Province, Argentina (Figure S2).

Diagnosis

Adult specimen with two openings within the antorbital fossa of the maxilla; jugal stepped along caudal edge of the postorbital process; postorbital with a low and rounded lateral horn on the squamosal process; lacrimal with rounded projections along its dorsal margin; quadratojugal with a deep and rounded fossa on its lateral surface; sacral vertebral neural spines almost completely co-ossified; anterior caudal vertebrae with complex hyposphene-hypantrum articulations; humerus with internal tuberosity separated from humeral head by a cleft and an ovoid fossa on its anteroproximal surface; strongly enlarged 2nd pedal claw, almost twice the length of the digit IV ungual (see STAR Methods for differential diagnosis).

Description and comparisons

The skull of *Meraxes* is long and low, with profusely ornamented dermal bones, and is similar in shape and proportions to that of Acrocanthosaurus. 12,13 The lateral surface of the maxilla is ornamented by irregular vertical furrows and ridges. The nasals are covered by well-developed rugosities and bumps except for the smooth anterolateral area that surrounds the external nares, as in other carcharodontosaurines. 7,9 The lacrimal is ornamented with ridges and furrows on its lateral surface and rounded projections along the dorsal margin. A robust brow horn projects laterally from the postorbital and is marked by a vascular horizontal groove extending across its lateral face as in other derived carcharodontosaurids.^{6,7} A dorsoventrally elongated ridge extends along the posterior edge of the quadrate

Report



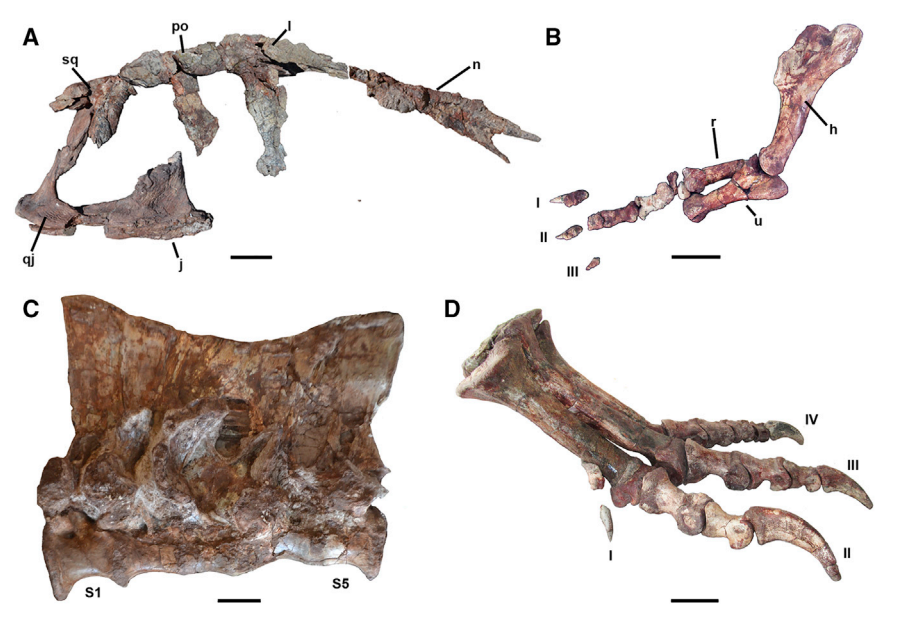


Figure 2. Meraxes gigas MMCh-PV 65, select

(A) Right side of the skull.

(B) Articulated right arm in medial view (I to III, hand digits, first to third).

(C) Sacrum in left lateral view (S1, first sacral; S5,

(D) Left foot in medial view (I to IV, pedal digits first to

h, humerus; j, jugal; l, lacrimal; n, nasal; qj, quadratojugal; po, postorbital; r, radius; sq, squamosal; u, ulna. Scale bars, 10 cm.

See also Figures S1 and S2 and Tables S1-S3.

the homolog of the avian attachment point for the acrocoracohumeral ligament. 17,18 The distal articulation is farther rotated with respect to the proximal end than in Acrocanthosaurus. 12

The ulna is short and stout. The olecranon process is block-shaped, forms 27% of the total length of the bone, and

has a trapezoidal outline in caudal view. A robust medioventral crest, which is also visible in proximal view as a medially directed tuberosity, is more prominent than in Allosaurus and Acrocanthosaurus. 12,14

Only metacarpals II and III were recovered. Both are robust bones with strongly expanded ends and almost flat proximal articular surfaces. Metacarpal II has a depression on the proximolateral corner for articulation with metacarpal III. The distal condyles of metacarpal II are asymmetrical in shape but not size, as in Acrocanthosaurus, 12 allowing the tip of the claw to rotate medially during flexion and laterally during hyperextension. The distal articular surface of metacarpal III is almost subspherical.

Nine manual phalanges were recovered. Phalanx I-1 is the longest and least expanded at the ends. Ungual phalanx I-2 is very robust and recurved with a strongly developed flexor tubercle that is larger than in Allosaurus. 14 The unguals of the other digits are similar in form but smaller. The size differences between the unguals are similar to Allosaurus. 14

In lateral view, the iliac blade is trapezoidal, as in Allosaurus, but proportionally shorter and taller. The pubic foramen is completely enclosed by bone, unlike the notch observed in other allosauroids. The ischial shaft is straight as in Acrocanthosaurus, unlike the curved shaft present in Mapusaurus.

The femur has a strongly upturned and slightly anteromedially oriented femoral head. The tibia has an anterodorsally projected cnemial crest, with a subrectangular outline in lateral view. The expanded proximal end of the fibula is excavated by an ovoid medial fossa, which is internally covered by low ridges in a cross-pattern, as also observed in Giganotosaurus and Mapusaurus.

The astragalus has a robust, hourglass-shaped body with a wide and relatively shallow horizontal groove extending along the condyles and onto the calcaneum. The height of the ascending process with respect to tibial length is a character with a long history in theropod systematics, but has not been known in carcharodontosaurids until now. Meraxes demonstrates

shaft and is sigmoid, unlike the straight ones in Acrocanthosaurus and Allosaurus. 13,14 The paired frontals are separated anteriorly by a "U-shaped" cleft for the articulation with nasals. As in Giganotosaurus and Carcharodontosaurus saharicus, 6,7 the parietal skull table is wide. The supraoccipital forms a conspicuous knob dorsally, though it is less prominent than in Giganotosaurus or Carcharodontosaurus. The paroccipital process is very long and more ventrally angled than in Acrocanthosaurus. 13 The basipterygoid processes are long, finger-like projections, which border a wide, triangular, and anteriorly enlarged subsellar recess. The parasphenoid-basisphenoid complex is included in the interorbital septum, which is fully ossified, as in Giganotosaurus and Carcharodontosarus. 15 The palatine is extensively pneumatized as in Neovenator and Acrocanthosaurus.

Five sacral vertebrae are co-ossified, not only through their centra but also between the neural spines. In other carcharodontosaurids like Acrocanthosaurus 16 and Giganotosaurus, some neural spines show partial co-ossification of their distal parts, but never to the degree seen in Meraxes. The sacral spine-table has a sigmoid profile with the anterior-most and posterior-most spines projecting above the iliac margin in lateral view.

Caudals 1-2 and 3-4 exhibit a degree of fusion between their neural spines. The postzygapophyses of the first four caudal vertebrae bear well-developed hyposphen-hypantrum articulations. The anterior caudal vertebrae bear marked pneumatic features on their neural arches and spines including wide and deep spinopostzygapophyseal fossae along the posterior base of the neural spines, in the first five. A pair of foramina open into these fossae behind the postzygapophyses. Some neural spine bases are indented laterally by wide pneumatic depressions.

The scapula is a long, robust, and gently curved bone. The coracoid shows a rounded outline with a well-developed posteroventral process. The humerus is stout and expanded at both ends. As in Acrocanthosaurus, 12 the maximum width of the proximal end is half the length of the bone. The most distinctive humeral feature is a deep, mediolaterally ovoid fossa located just below the humeral head on the anterior side that could represent



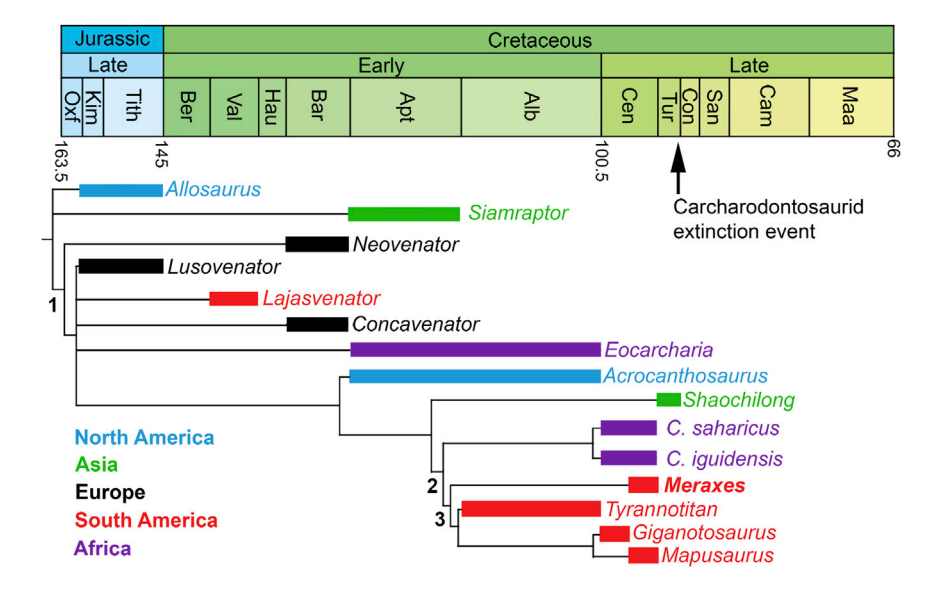


Figure 3. Cladogram depicting phylogenetic position of Meraxes gigas inside Allosauroidea, scaled with part of the Mesozoic time scale

Thick colored bars represent the stratigraphic resolution for each taxon, and the color of each bar indicates their geographic provenance. Clade names: 1. Carcharodontosauridae: 2. Carcharodontosaurinae; 3, Giganotosaurini. See also STAR Methods and Data S1.

that the astragalar ascending process is much less than one-sixth the length of the tibia. Meraxes also substantiates the more robust development of the calcaneum in carcharodontosaurids. Calcaneum width in Allosaurus and Sinraptor is 24% and 29% of the greatest width of the astragalus, respectively. 19 In Acrocanthosaurus the maximum width of the calcaneum represents 33% of the astragalus width, whereas in Meraxes it represents 36%.

Metatarsal III is the longest; metatarsals II and IV are subequal; metatarsal V is shorter, splint-like, and curved; and metatarsal I is the shortest. Metatarsal V articulates with the posterior surface of metatarsal IV. As is typical for theropods, all phalanges, with the exception of the II-2, have conspicuous extensor fossae on their dorsal surfaces next to their distal articular surfaces. Ungual III-4 is about 30% smaller than II-3, and IV-5 is 45% smaller than II-3. Besides being the largest of the feet, ungual II-3 shows a moderately sharp ventral edge, different from the rounded surface observed in the remaining unguals. Meraxes has very similar foot proportions to Acrocanthosaurus and Concavenator (digit III length/femoral length close to 0.40).

DISCUSSION

Phylogenetic analysis (STAR Methods; Data S1) recovers Meraxes as the earliest diverging member of the Giganotosaurini, a "mid" Cretaceous clade of South American gigantic (body mass > 4 tons) carcharodontosaurids (Figure 3). The addition of yet another species of giant carcharodontosaurid (body mass estimated: 4,263 kg; STAR Methods) from the lower part of the Huincul Formation, possibly coeval with Taurovenator,5 and stratigraphically intermediate between Giganotosaurus from the underlying Candeleros Formation and Mapusaurus from younger levels of the Huincul Formation, is further indication of the high diversity of this clade shortly before its extinction by Turonian-Coniacian times. 8,20 A comparable diversity of large tyrannosaurids is known from the Campanian of western North America.²¹ Despite their temporal and geographical proximity, Meraxes is readily distinguished from other Giganotosaurini by a suite of characters from throughout the skull and skeleton, including unique protuberances and rugosity patterns on the

dermal cranial bones. At a minimum, these differences suggest great lability and increased rates of trait evolution in facial ornamentation that may have had a social signaling role.22

Meraxes has the most complete cranium of any Carcharodontosaurinae, with a total skull length estimated at

127 cm, which is comparable to the most complete specimen of Acrocanthosaurus with a 123 cm skull. 12 Giganotosaurus has the next most complete skull among carcharodontosaurids, but it is missing part of the maxilla and several bones of the temporal series, rendering previous attempts to estimate its length uncertain and ranging from 156 to 180 cm.^{23,24} Scaling up the missing bones from *Meraxes* provides an estimate of \sim 162 cm for Giganotosaurus (STAR Methods), making it one of the longest theropod skulls yet discovered.

Meraxes is the only Late Cretaceous carcharodontosaurid to preserve near-complete forelimbs, which are only about half the length of the femur (47%), comparable to both later diverging tyrannosaurids and abelisaurids (Figure 4). Using quantitative tests of evolutionary convergence²⁵ (STAR Methods), we found that tyrannosaurids, abelisaurids, and carcharodontosaurids exhibit greater similarities in fore- to hindlimb ratios than would be expected under a Brownian motion evolutionary model (mean p < 0.01), and the degree of convergence is especially pronounced between Meraxes and the tyrannosauroid Tarbosaurus (mean p < 0.05) (Figure 4A). The degree of convergence is not as pronounced between Meraxes and the shortest armed abelisaurid in our sample, Carnotaurus, but is still significantly more similar than expected (mean p < 0.05). The degree of convergence in arm reduction across large-bodied theropods is less pronounced when looking at individual limb segments rather than the forelimb as a whole, but remains significant (p < 0.05) for the pairing of Tarbosaurus and Meraxes and near-significant for other comparisons. It is worth noting that this similarity is achieved despite the very different growth strategies recovered from histological analyses of Meraxes and tyrannosaurids.²⁶

This remarkable degree of convergence provides evidence that forelimb reduction was actively selected for in multiple lineages of large predatory theropods that independently evolved to occupy a distinct limb-size morphospace region (Figure 4B). Although all three short-armed lineages together define their own region of this morphospace, it is worth noting that there is little overlap between them. Much of the variance within and between these clades is observed in femur length, which is a proxy

Current Biology Report



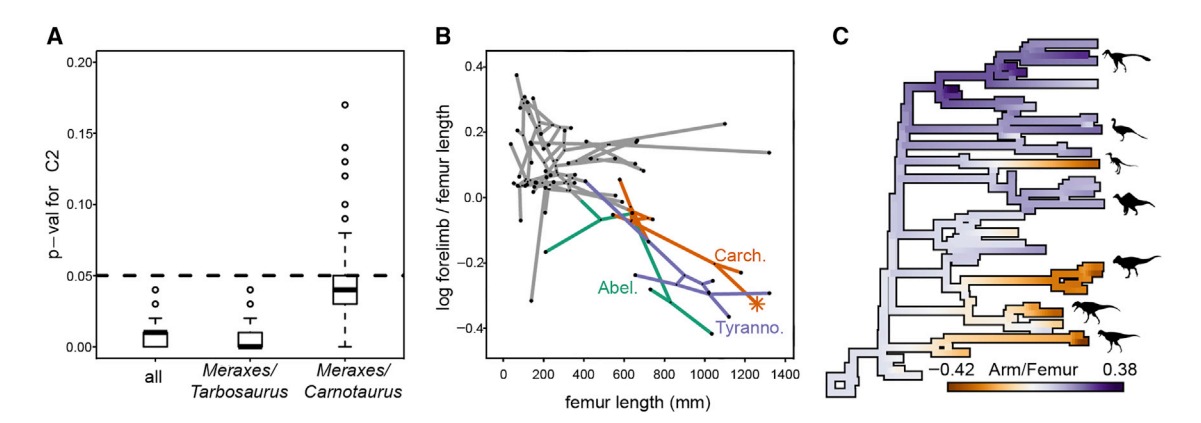


Figure 4. Arm reduction convergence analysis in Theropoda

(A) Results of significance testing using random resampling procedures on Stayton's²⁵ C₂ metric, which evaluates the degree of convergence between two terminals in a phylomorphospace (shown in B). Characters were assumed to evolve under a Brownian Motion model.

(B) Phylomorphospace of femur length (a proxy of body size) on the x axis and forelimb/femur length ratio (natural log scale) on the y axis for select theropods. Short-armed, large-bodied predatory species belonging to the Abelisauridae, Carcharodontosauridae, and Tyrannosauridae occupy a unique quadrant on the lower right. *Meraxes* indicated with an arrow.

(C) Forelimb/femur ratio traced as a continuous trait (ML optimization using Mk model) on the phylogenetic tree used in the analysis of convergence. Similar degrees of forelimb reduction evolved independently in 4 lineages: Abelisauridae, Carcharodontosauridae, Tyrannosauridae, and Alvarezsauridae. See also STAR Methods and Table S4.

for body size, rather than relative limb proportions, which track within a narrow range (0.6 > forelimb/femur > 0.4) (Figures 4B and 4C). This lack of overlap between the three groups suggests that the forelimb reduction is not simply a result of a common allometric pattern with arm reduction tracking absolute body size, but rather represents a suite of similar though not necessarily identical allometries. It is worth noting that the early diverging members of Abelisauroidea and Allosauroidea, including Eoabelisaurus, Concavenator, and Allosaurus, are more closely clustered in morphospace than are the laterdiverging members of either lineage, or later diverging tyrannosaurids for that matter. This variance is at least partially explained by clades evolving smaller forelimb/femur ratios over time somewhat independent of size as, for example, demonstrated by the proportionately shorter forelimb of Meraxes when compared to Acrocanthosaurus, although both were very similar in size.

Our quantitative analyses provide further substantiation that parallel allometric trends may be responsible for changes in fore- to hindlimb ratios in some theropods, but we also emphasize that the forelimb-hindlimb ratios do not co-vary tightly with size even among closely related species of very large predatory theropods. The underlying causes for this variance may relate to multiple factors including greater variance in forelimb length and how much each of the three developmental segments contribute to arm length in short-armed taxa, perhaps associated with a loosening of developmental constraints as a result of reduction or change in function. To explain how these three lineages arrive at remarkably similar degrees of arm reduction despite the variance within each lineage, we propose that a lower bound, or constraint, exists around a forelimb/femur ratio of 0.4 with respect to the degree of arm reduction that can be achieved evolutionarily. This ratio is approached or met not only in the three large-bodied clades we focus on here, but is also approximated in derived members of much smaller-bodied lineages including the parvicursorine alvarezsaurid *Mononykus* and the noasaurid *Limusaurus* (Figures 4B and 4C). The degree of forelimb shortening does not necessarily correlate with robustness and musculature of the forelimb.²⁷ In *Meraxes*, as in tyrannosaurids (and alvarezsaurids), the forelimb bones are robust and exhibit prominent muscle attachments including the deltopectoral crest and internal and external epicondyles, whereas muscle attachment processes are strongly reduced in abelisaurids and noasaurids, as well as in ratites.^{27–29}

Historically, there has been great interest in inferring the potential functions of the proportionately diminutive limbs in large theropods like *T. rex.* with interpretations including reproductive behavior, body support when an animal is rising from a prone position, 30,31 or predatory behavior. 32,33 Other authors have considered the forelimbs of tyrannosaurids and abelisaurids as vestigial with limited or no function, 34-36 whereas a third school of thought has been to distinguish the question of function in individual species from macroevolutionary processes that may account for arm reduction in these species perhaps as a result of selection for other traits.^{37–39} Our study provides some support for the latter hypothesis with similar proportions observed in unrelated large predatory theropod lineages. The presence of multi-ton theropods with long forelimbs, but small skulls, such as the ornithomimosaur Deinocheirus and the caenagnathid Gigantoraptor, further confirms that forelimb reduction is not a simple function of body size in theropods, but rather that it tracks some other trait, which for large predatory species is likely skull size. 37,39 Phylogenetic regressions appear to bear this out, as skull size requires a negative interaction with femur length to accurately predict arm length⁴⁰ (STAR Methods).

STAR***METHODS**

Detailed methods are provided in the online version of this paper and include the following:



Current BiologyReport

- KEY RESOURCES TABLE
- RESOURCE AVAILABILITY
 - Lead contact
 - Materials availability
 - Data and code availability
- EXPERIMENTAL MODEL AND SUBJECT DETAILS
- METHOD DETAILS
 - Phylogenetic analysis
 - Histological analysis
 - Technical details on the fieldwork and extraction activities
 - Nomenclatural acts
- QUANTIFICATION AND STATISTICAL ANALYSIS
 - O Body mass estimation
 - Analysis on skull dimensions in Giganotosaurus
 - Convergence analysis

SUPPLEMENTAL INFORMATION

Supplemental information can be found online at https://doi.org/10.1016/j.cub.2022.05.057.

ACKNOWLEDGMENTS

The authors would like to thank to Eduardo Ruigómez, Rodolfo Coria, Jorge Calvo, Mike Getty, Vince Schneider, and Paul Sereno for allowing the access to specimens under their care. The collection visit to the USA was possible thanks to a grant from the Jurassic Foundation (to J.I.C.). Many thanks to Dr. Stephen Brusatte and an anonymous reviewer for their useful comments on the manuscript. The program TNT is made freely available, thanks to a subsidy by the Willi Hennig Society. Field operations and research were funded by The National Geographic Society, Municipalidad de Villa El Chocón, Fundación "Félix de Azara," The Field Museum, and Agencia I+D+i (PICT 2018-04042). We wish to thank the participants in the fieldwork and the preparators who worked of the specimen: Rogelio Zapata, Javier Pazo, Andrés Moretti, Jonatan Aroca, Leandro Ripoll, Christian Albornoz, Mara Ripoll, Natalia Gonzalez, Frank Endress, Agustín Pérez Moreno, Ignacio Maniel, Jorge Bolomey, Mauricio Cerroni, Guillermina Giordano, Damián Amarilla, Carlos Corral, Iñaki Guaycochea, Manuel Negrón, and Matt Lewin. Thanks to Damiano Palombi for his help and discussions in the final stage of the manuscript. Mr. Pedro Lucero is thanked for his logistical help with his vehicle. We also thank the Zarza family and Luis Perouene for kindly allowing access to their property. Lynnea Jackson compiled measurement data for the phylogenetic comparative analyses. P.J.M. acknowledges funding from the US National Science Foundation FRES 1925884.

AUTHOR CONTRIBUTIONS

J.I.C., S.A., P.A.G., J.M., N.D.S., T.M.C., A.S., A.H., F.A.G., and P.J.M. designed and performed research; J.M., T.M.C., A.H., and P.J.M. contributed new reagents/analytic tools; J.I.C., J.M., T.M.C., A.H., and P.J.M. analyzed data; and J.I.C., S.A., P.A.G., J.M., N.D.S., T.M.C., A.S., A.H., F.A.G., and P.J.M. wrote the paper.

DECLARATION OF INTERESTS

The authors declare no competing interests.

Received: February 10, 2022 Revised: April 8, 2022 Accepted: May 25, 2022 Published: July 7, 2022

REFERENCES

- Osborn, H.F. (1906). Tyrannosaurus, Upper Cretaceous carnivorous dinosaur (second communication). Bull. Am. Mus. Nat. Hist. 22, 281–296.
- Bonaparte, J.F., Novas, F.E., and Coria, R.A. (1990). Carnotaurus sastrei
 Bonaparte, the horned, lightly built, carnosaur from the middle
 Cretaceous of Patagonia. Contrib. Sci. (Los Angel.) 416, 1–42.
- Stovall, J.W., and Langston, W. (1950). Acrocanthosaurus atokensis, a new genus and species of Lower Cretaceous Theropoda from Oklahoma. Am. Midl. Nat. 43, 696–728.
- Ortega, F., Escaso, F., and Sanz, J.L. (2010). A bizarre, humped Carcharodontosauria (Theropoda) from the Lower Cretaceous of Spain. Nature 467, 203–206. https://doi.org/10.1038/nature09181.
- Coria, R.A., Currie, P.J., Ortega, F., and Baiano, M.A. (2020). An Early Cretaceous, medium-sized carcharodontosaurid theropod (Dinosauria, Saurischia) from the Mulichinco Formation (upper Valanginian), Neuquén Province, Patagonia, Argentina. Cretac. Res. 111, 104319. https://doi. org/10.1016/j.cretres.2019.104319.
- Coria, R.A., and Salgado, L. (1995). A new giant carnivorous dinosaur from the Cretaceous of Patagonia. Nature 377, 224–226.
- Sereno, P.C., Dutheil, D.B., Iarochene, M., Larsson, H.C., Lyon, G.H., Magwene, P.M., Sidor, C.A., Varrichio, D.J., and Wilson, J.A. (1996). Predatory dinosaurs from the Sahara and Late Cretaceous faunal differentiation. Science 272, 986–991.
- Novas, F.E., de Valais, S., Vickers Rich, P., and Rich, T. (2005). A large Cretaceous theropod from Patagonia, Argentina, and the evolution of carcharodontosaurids. Naturwissenschaften 92, 226–230. https://doi. org/10.1007/s00114-005-0623-3.
- Coria, R.A., and Currie, P.J. (2006). A new carcharodontosaurid (Dinosauria, Theropoda) from the Upper Cretaceous of Argentina. Geodiversitas 28, 71–118.
- Motta, M., Aranciaga Rolando, A.M., Rozadilla, S., Agnolín, F.E., Chimento, N.R., Brissón Egli, F., and Novas, F.E. (2016). New theropod fauna from the Upper Cretaceous (Huincul Formation) of northwestern Patagonia, Argentina. Bull. N. M. Mus. Nat. Hist. Sci. 71, 231–253.
- Garrido, A.C. (2010). Estratigrafía del Grupo Neuquén, Cretácico Superior de la Cuenca Neuquina (Argentina): nueva propuesta de ordenamiento litoestratigráfico. Rev. Mus. Arg. Cs. Nat. n.s. 12, 121–177.
- Currie, P.J., and Carpenter, K. (2000). A new specimen of Acrocanthosaurus atokensis (Theropoda, Dinosauria) from the Lower Cretaceous Antlers Formation (Lower Cretaceous, Aptian) of Oklahoma, USA. Geodiversitas 22, 207–246.
- Eddy, D., and Clarke, J. (2011). New information on the cranial anatomy of Acrocanthosaurus atokensis and its implications for the phylogeny of Allosauroidea (Dinosauria: Theropoda). PLoS One 6, e17932.
- Madsen, J.H. (1976). Allosaurus fragilis: a revised osteology. Utah Geol. Mineralog. Survey Bull. 10, 3–163.
- Coria, R.A., and Currie, P.J. (2002). The braincase of *Giganotosaurus carolinii*, (Dinosauria: Theropoda) from the Upper Cretaceous of Argentina. J. Vertebr. Paleontol. 4, 802–811. https://doi.org/10.1671/0272-4634(2002)022[0802:TBOGCD]2.0.CO;2.
- Harris, J.D. (1998). A reanalysis of Acrocanthosaurus atokensis, its phylogenetic status and paleobiogeographic implications, based on a new specimen from Texas. Bull. N. M. Mus. Nat. Hist. Sci. 13, 1–75.
- Baumel, J.J., and Witmer, L.M. (1993). Osteologia. In Handbook of Avian Anatomy: Nomina Anatomica Avium, Second Edition, J.J. Baumel, A.S. King, J.E. Breazile, H.E. Evans, and J.C. Vanden Berge, eds. (Publications of the Nuttall Ornithological Club 23), pp. 45–132.
- 18. Baumel, J.J., and Raikow, R.J. (1993). Arthrologia. In Handbook of Avian Anatomy: Nomina Anatomica Avium, Second Edition, J.J. Baumel, A.S. King, J.E. Breazile, H.E. Evans, and J.C. Vanden Berge, eds. (Publications of the Nuttall Ornithological Club 23), pp. 133–188.

Report



- 19. Currie, P.J., and Zhao, X. (1993). A new carnosaur (Dinosauria, Theropoda) from the Jurassic of Xinjiang, People's Republic of China. Can. J. Earth Sci. 30, 2037-2081.
- 20. Novas, F.E., Agnolín, F.L., Ezcurra, M.D., Porfiri, J.D., and Canale, J.I. (2013). Evolution of the carnivorous dinosaurus during the Cretaceous: the evidence from Patagonia. Cretac. Res. 45, 174-215. https://doi.org/ 10.1016/j.cretres.2013.04.001.
- 21. Carr, T.D., Williamson, T.E., Britt, B.B., and Stadtman, K. (2011). Evidence for high taxonomic and morphologic tyrannosauroid diversity in the Late Cretaceous (Late Campanian) of the American Southwest and a new short-skulled tyrannosaurid from the Kaiparowits formation of Utah. Naturwissenschaften 98, 241-246. https://doi.org/10.1007/s00114-011-
- 22. Gates, T., Organ, C., and Zanno, L. (2016). Bony cranial ornamentation linked to rapid evolution of gigantic theropod dinosaurs. Nat. Commun. 7, 12931. https://doi.org/10.1038/ncomms12931.
- 23. Thérrien, F., and Henderson, D.M. (2007). My theropod is bigger than yours... or not: estimating body size from skull length in theropods. J. Vertebr. Paleontol. 27, 108-115. https://doi.org/10.1671/0272-4634(2007)27[108:MTIBTY]2.0.CO;2.
- 24. Calvo, J.O., and Coria, R.A. (2000). New specimen of Giganotosaurus carolinii (Coria and Salgado, 1995), supports it as the largest theropod ever found. Gaia 15, 117-122.
- 25. Stayton, C.T. (2015). The definition, recognition, and interpretation of convergent evolution, and two new measures for quantifying and assessing the significance of convergence. Evolution 69, 2140-2153. https://doi. org/10.1111/evo.12729.
- 26. Cullen, T.M., Canale, J.I., Apesteguía, S., Smith, N.D., Hu, D., and Makovicky, P.J. (2020). Osteohistological analyses reveal diverse strategies of theropod dinosaur body- size evolution. Proc. Roy. Soc. Lond. B. 287, 2258. https://doi.org/10.1098/rspb.2020.2258.
- 27. Apesteguía, S., Smith, N.D., Juárez Valieri, R., and Makovicky, P.J. (2016). An unusual new theropod with a didactyl manus from the Upper Cretaceous of Patagonia, Argentina. PLoS One 11, e0157793. https:// doi.org/10.1371/journal.pone.0157793.
- 28. Burch, S.H. (2017). Myology of the forelimb of Majungasaurus crenatissimus (Theropoda, Abelisauridae) and the morphological consequences of extreme limb reduction. J. Anat. 231, 515-531. https://doi.org/10.1111/
- 29. Maxwell, E.E., and Larsson, H.C.E. (2007). Osteology and myology of the wing of the emu (Dromaius novaehollandiae), and its bearing on the evolution of vestigial structures. J. Morphol. 268, 423-441. https://doi.org/10. 1002/jmor.10527.
- 30. Newman, B.H. (1970). Stance and gait in the flesh-eating dinosaur Tyrannosaurus. Biol. J. Linn. Soc. 2, 119-123. https://doi.org/10.1111/j. 1095-8312.1970.tb01707.x.
- 31. Stevens, K.A., Larson, P., Willis, E.D., and Anderson, A. (2008). Rex, sit: digital modelling of Tyrannosaurus rex at rest. In Tyrannosaurus rex, the Tyrant King, P. Larson, and K. Carpenter, eds. (Indiana University Press), pp. 193-203.
- 32. Carpenter, K., and Smith, M. (2001). Forelimb osteology and biomechanics of Tyrannosaurus rex. In Mesozoic Vertebrate Life, D.H. Tanke, and K. Carpenter, eds. (Indiana University Press), pp. 90-116.
- 33. Lipkin, C., and Carpenter, K. (2008). Looking again at the forelimb of Tyrannosaurus rex. In Tyrannosaurus rex, the Tyrant King, P. Larson, and K. Carpenter, eds. (Indiana University Press), pp. 176-192.
- 34. Paul, G.S. (1988). Predatory Dinosaurs of the World (Simon & Schuster).
- 35. Fastovsky. D.E., and Weishampel, D.B. (2005). The Evolution and Extinction of the Dinosaurs (Cambridge Univ. Press).
- 36. Horner, J.R., and Lessem, D. (1993). The Complete T. rex: How Stunning New Discoveries Are Changing Our Understanding of the World's Most Famous Dinosaur (Simon & Schuster).

- 37. Gould, S.J., and Lewontin, R.C. (1979). The spandrels of San Marco and the Panglossian paradigm: a critique of the adaptationist programme. Proc. Roy. Soc. Lond. B. 205, 581-598.
- 38. Guinard, G. (2020). Forelimb shortening of Carcharodontosauria (Dinosauria: Theropoda): an update on evolutionary anterior micromelias in non-avian theropods. Zoology 139, 125756. https://doi.org/10.1016/j. zool.2020.125756.
- 39. Lockley, M., Kuhihara, R., and Mitchell, L. (2008). Why Tyrannosaurus rex had puny arms: An integral morphodynamic solution to a simple puzzle in Theropod Paleobiology. In *Tyrannosaurus rex*, the Tyrant King, P. Larson, and K. Carpenter, eds. (Indiana University Press), pp. 130-164.
- 40. Ho, L.S.T., and Ane, C. (2014). A linear-time algorithm for Gaussian and non-Gaussian trait evolution models. Syst. Biol. 63, 397-408. https://doi. org/10.1093/sysbio/syu005.
- 41. Canale, J.I., Novas, F.E., and Pol, D. (2015). Osteology and phylogenetic relationships of Tyrannotitan chubutensis Novas, de Valais, Vickers-Rich and Rich 2005 (Theropoda: Carcharodontosauridae) from the Lower Cretaceous of Patagonia, Argentina. Hist. Biol. 27, 1-32. https://doi.org/ 10.1080/08912963.2013.861830.
- 42. Chokchaloemwong, D., Hattori, S., Cuesta, E., Jintasakul, P., Shibata, M., and Azuma, Y. (2019). A new carcharodontosaurian theropod (Dinosauria: Saurischia) from the Lower Cretaceous of Thailand. PLoS One 14, e0222489. https://doi.org/10.1371/journal.pone.0222489.
- 43. Malafaia, E., Mocho, P., Escaso, F., and Ortega, F. (2020). A new carcharodontosaurian theropod from the Lusitanian Basin: evidence of allosauroid sympatry in the European Late Jurassic. J. Vertebr. Paleontol. 40, e1768106. https://doi.org/10.1080/02724634.2020.1768106.
- 44. Cuesta, E., Ortega, F., and Sanz, J.L. (2018). Appendicular osteology of Concavenator corcovatus (Theropoda: Carcharodontosauridae) from the Lower Cretaceous of Spain. J. Vertebr. Paleontol. 38, 1-24. https://doi. org/10.1080/02724634.2018.1485153.
- 45. Goloboff, P.A., and Catalano, S.A. (2016). TNT version 1.5, including a full implementation of phylogenetic morphometrics. Cladistics 32, 221-238. https://doi.org/10.1111/cla.12160.
- 46. Werning, S. (2012). The ontogenetic osteohistology of Tenontosaurus tilletti. PLoS One 7. e33539
- 47. Prondvai, E., Stein, K.H., de Ricqlès, A., and Cubo, J. (2014). Development-based revision of bone tissue classification: the importance of semantics for science. Biol. J. Linn. Soc. 112, 799-816. https://doi.org/ 10.1111/bij.12323.
- 48. Jin, X., Varricchio, D.J., Poust, A.W., and He, T. (2020). An oviraptorosaur adult-egg association from the Cretaceous of Jiangxi Province, China. J. Vertebr. Paleontol. 39, e1739060.
- 49. Cullen, T.M., Brown, C.M., Chiba, K., Brink, K.S., Makovicky, P.J., and Evans, D.C. (2021). Growth variability, dimensional scaling, and the interpretation of osteohistological growth data. Biol. Lett. 17, 20210383.
- 50. Koob, S.P. (1986). The use of Paraloid B-72 as an adhesive: its application for archaeological ceramics and other materials. Stud. Conserv. 31, 7–14.
- 51. Campione, N.E., Evans, D.C., Brown, C.M., and Carrano, M.T. (2014). Body mass estimation in non-avian bipeds using a theoretical conversion to quadruped stylopodial proportions. Methods Ecol. Evol. 5, 913-923. https://doi.org/10.1111/2041-210X.12226.
- 52. Campione, N.E. (2020). MASSTIMATE: Body Mass Estimation Equations for Vertebrates. R package version 2.0-1. https://CRAN.R-project.org/ package=MASSTIMATE.
- 53. Lee, Y.N., Barsbold, R., Currie, P.J., Kobayashi, Y., Lee, H.J., Godefroit, P., Escuillié, F., and Chinzorig, T. (2014). Resolving the long-standing enigmas of a giant ornithomimosaur Deinocheirus mirificus. Nature 515, 257-260. https://doi.org/10.1038/nature13874.
- 54. Brochu, C.A. (2003). Osteology of Tyrannosaurus rex: insights from a nearly complete skeleton and high-resolution computed tomographic analysis of the skull. J. Vertebr. Paleontol. 22, 1-138. https://doi.org/10. 1080/02724634.2003.10010947.



Current Biology

- 55. Carrano, M.T., Benson, R.B., and Sampson, S.D. (2012). The phylogeny of tetanurae (Dinosauria: Theropoda). J. Syst. Palaeontol. 10, 211-300. https://doi.org/10.1080/14772019.2011.630927.
- 56. Hendrickx, C., and Mateus, O. (2014). Torvosaurus gurneyi n. sp., the largest terrestrial predator from Europe, and a proposed terminology of the maxilla anatomy in nonavian theropods. PLoS One 9, e88905. https://doi.org/10.1371/journal.pone.0088905.
- 57. Sasso, C.D., Maganuco, S., Buffetaut, E., and Mendez, M.A. (2005). New information on the skull of the enigmatic theropod Spinosaurus, with remarks on its size and affinities. J. Vertebr. Paleontol. 25, 888-896. https://doi.org/10.1671/0272-4634(2005)025[0888:NIOTSO]2.0.CO;2.
- 58. Ibrahim, N., Sereno, P.C., Varricchio, D.J., Martill, D.M., Dutheil, D.B., Unwin, D.M., Baidder, L., Larsson, H.C.E., Zouhri, S., and Kaoukaya, A. (2020). Geology and paleontology of the Upper Cretaceous Kem Kem Group of eastern Morocco. ZooKeys 928, 1-216. https://doi.org/10. 3897/zookeys.928.47517.

- 59. Bapst, D.W. (2013). A stochastic rate-calibrated method for time-scaling phylogenies of fossil taxa. Methods Ecol. Evol. 4, 724-733. https://doi. org/10.1111/2041-210X.12081.
- 60. Castiglione, S., Serio, C., Mondanaro, A., Melchionna, M., Carotenuto, F., Febbraro, M.D., Profico, A., Tamagini, D., and Raia, P. (2020). Ancestral state estimation with phylogenetic ridge regression. Evol. Biol. 47, 220-232. https://doi.org/10.1007/s11692-020-09505-x.
- 61. Revell, L.J. (2009). Size-correction and principal components for interspecific comparative studies. Evolution 63, 3258-3268. https://doi.org/10. 1111/j.1558-5646.2009.00804.x.
- 62. Revell, L.J. (2012). Phytools: an R package for phylogenetic comparative biology (and other things). Methods Ecol. Evol. 63, 3258-3268.
- 63. Benson, R.B.G., and Choiniere, J.N. (2013). Rates of dinosaur limb evolution provide evidence for exceptional radiation in Mesozoic birds. Proc. Biol. Sci. 280, 1768. https://doi.org/10.1098/rspb.2013.1780.

Current Biology Report



STAR***METHODS**

KEY RESOURCES TABLE

Holotype specimen of Meraxes gigas	This paper	MMCh-PV 65
Other		
Microsoft Excel	http://www.microsoft.com/en-us/	N/A
R package "MASSTIMATE"	https://cran.r-project.org/package=MASSTIMATE	N/A
R programming language, ver 4.1.0	https://cran.r-project.org	N/A
TNT: Tree Analysis using New Technology	http://www.lillo.org.ar/phylogeny/tnt/	N/A
Software and algorithms		
Convergence analysis data	https://doi.org/10.5061/dryad.r7sqv9sfp	https://doi.org/10.5061/dryad.r7sqv9sfp
Convergence analysis, table of simulation means and standard deviations	This paper	Data S3
Giganotosaurus skull dimension analysis	This paper	Data S2
Phylogenetic data matrix	This paper	Data S1
Deposited data		
REAGENT or RESOURCE	SOURCE	IDENTIFIER

RESOURCE AVAILABILITY

Lead contact

Further information and requests for resources and reagents should be directed to and will be fulfilled by the lead contact Dr. Juan Ignacio Canale (jicanale@unrn.edu.ar).

Materials availability

The authors declare that the specimen MMCh-PV 65, which is the focus of this study is housed at the Museo Paleontológico "Ernesto Bachmann", Neuquén, Argentina.

Data and code availability

The authors declare that all data generated or analyzed during this study are included in this published article, the Supplemental information or at the Data S1, S2, and S3 files and on Dryad https://doi.org/10.5061/dryad.r7sqv9sfp.

EXPERIMENTAL MODEL AND SUBJECT DETAILS

The data used for anatomical comparisons and phylogenetic analysis in this study was collected both from the literature and first-hand examination of the following fossil specimens housed in public trust repositories:

- Acrocanthosaurus atokensis North Carolina State Museum of Natural Sciences, Raleigh, North Carolina. NCSM 14345.
- Allosaurus fragilis Utah Museum of Natural History, Utah. UMNH-VP 13812, 7437, 6504, 9248, 9168, 9218, 9211, 9351, 6476, 9185, 9180, 9323, 9296, 9295, 9379, 9191, 8879, 5328, 9311, 9085, 9086, 8972, 8944, 8946, 9569, 9500, 8950, 8953, 9473, 9472, 8925, 5437, 9150, 9142, 9100, 9103, 9135, 7812, 8846, 5480, 7756, 3109, 8484, 8519, 5685, 8487, 8355, 8354, 8397, 5145, 10129, 10067, 10068, 10069, 10259, 7414, 7409, 8515, 8334, 9018, 10108, 10109, 9019, 8799, 8697, 8725, 9003, 90227, 10091, 10089, 10092, 8574, 5278, 9822, 5411, 8245, 10127, 10126, 8151, 8157, 8146, 9722, 9718, 5410, 8100, 1152, 12231, 7928, 6400, 9402, 10142, 9931, 5682, 5348, 10017; UUVP 1852, 40-273.
- Carcharodontosaurus iguidensis DINOLAB, University of Chicago, Chicago, MNN IGU 2, 3, 4, 5, 6, 7, 8, 9, 10.
- Carcharodontosaurus saharicus DINOLAB, University of Chicago, Chicago. SGM-Din 1. North Carolina State Museum of Natural Sciences, Raleigh, North Carolina. NCSM 18166 (Replica).
- Eocarcharia dinops DINOLAB, University of Chicago, Chicago. MNN GAD2, 3, 4, 5, 6, 10, 11, 13, 14, 15.
- Giganotosaurus carolinii Museo Paleontológico "Ernesto Bachmann", Villa El Chocón, Neuquén MUCPv-CH 1 (Holotype).
 Museo de Geología y Paleontología, Universidad Nacional del Comahue, (Centro Paleontológico Lago Barreales), Neuquén MUC-Pv 95 (Referred specimen).
- Mapusaurus roseae Museo Municipal "Carmen Funes", Plaza Huincul, Neuquén. MCF-PVPH 108 (Holotype).
- Tyrannotitan chubutensis Museo Paleontológico "Egidio Feruglio", Trelew, Chubut. MPEF-PV 1156 (Holotype); MPEF-PV 1157 (Paratype).





METHOD DETAILS

Phylogenetic analysis

The phylogenetic analysis is based on the data matrix published by Canale et al., 41 to which the recently published taxa Lajasvenator ascheriae, 5 Siamraptor suwati, 42 and Lusovenator santosi, 43 the following additional characters were added:

Character 170: Nasal: central lateral expansion covering the antorbital fossa dorsolaterally (New). 0: Absent, 1: Present. Carcharodontosaurid nasals are usually ornamented with strong protuberances over the main bone surface, especially in more derived forms. In South American taxa, like Giganotosaurus, Mapusaurus and Meraxes, the nasal also shows a strong lateral widening on its central sector, profusely covered by rounded protuberances, which can be clearly observed in dorsal view. These protuberances, which are clearly absent in other allosauroids like Carcharodontosaurus or Acrocanthosaurus, cover the large and rounded pneumatopores, located on its ventral surface dorsally and laterally.

Character 171: Posterior projection of the parietals over the supraoccipital (New). 0: Absent, 1: Present, triangular, 2: Present, tongue-like. In some derived carcharodontosaurids the posterodorsal sector of the occipital plate shows a pronounced supraoccipital knob, which is covered dorsally by a posterior projection of the parietal. In the case of Carcharodontosaurus saharicus this projection shows a clear triangular outline in dorsal view, whereas in Giganotosaurus and Meraxes the same projection has a rounded, tongue-like contour.

Character 172: Scapula, distinct proximal neck in lateral view (New). 0: Absent, 1: Present. In basal allosauroids, like Allosaurus, Concavenator or Sinraptor the scapular blade dorsal and ventral margins are nearly straight throughout their lengths, with no discernible change in the dorsoventral height at any sector. In the case of Acrocanthosaurus, Giganotosaurus, Mapusaurus and Meraxes, the proximal section of the scapular blade shows a decrease in its dorsoventral height, forming a "neck" just before the proximal expansion which contacts the coracoid. This neck occupies about the first quarter of the blade and has a rounded ventral margin, whereas the remaining length of this margin is sharp.

Character 173: Humeral head, connection to greater tuberosity (From Cuesta et al. 44). 0: Confluent with the greater tuberosity, 1: Separated by an anteroposterior concavity.

Character 174: Ilium, concavity over the anterior margin of the iliac blade (New). 0: Absent, 1: Present. In some allosauroids, like Allosaurus, Sinraptor, Monolophosaurus and Mapusaurus the cranial or anterior margin of the iliac blade is straight or slightly convex. In Concavenator and Meraxes the dorsal sector of this margin shows a large concavity, clearly observable in lateral view. Cuesta et al. 44 proposed the possibility that in the case of Concavenator this concavity could be an incomplete, broken edge. Given it is also present in Meraxes, it is likely an anatomical feature.

Character 175: Astragalus, shape of ascending process. (New) 0: Triangular, 1: Trapezoidal. The astragalus is not commonly preserved in derived allosauroids, and is only complete in a few basal species. The astragalar ascending process, when present, shows two different shapes. In basal forms, like Allosaurus and Sinraptor it shows a triangular outline, with a pointed tip, while in Concavenator and Meraxes the the ascending process shows a trapezoidal shape, with a truncated tip.

Also, several character scorings in the original matrix were corrected (Data S1). The data matrix was analyzed in TNT (ver. 1.5). 45 A traditional search was implemented with 1000 replications saving 1000 trees per replication, and using Tree Bisection Reconnection as a swapping algorithm. Six most-parsimonious tres (MPTs) were recovered, each with a length of 338, a Consistency Index of 0.601 and a Retention Index of 0.743. The strict consensus tree (CI: 0.577, RI: 0.716) shows Meraxes deeply nested in Carcharodontosauridae, as the basalmost Giganotosaurini. The latter clade is diagnosed in this analysis by five synapomorphies: maxilla, medial view, termination of palatal suture anterior to distal margin of tooth seven (char. 22:0), Jugal, postorbital process wide based, process height less than twice the lenght of the base (char. 50:0), caudal vertebrae, pneumatic openings absent or as shallow fossae on the lateral sides of the centrum (char. 130: 0), Nasal: central widening covering the antorbital fossa dorsolaterally (char. 170:1), Tongue-like posterior projection of the parietals over the supraoccipital (char. 171: 2).

Histological analysis

Osteohistological thin-sections were produced from a wedge of the rigth femur (taken on the anterior at approximately mid-shaft), a transverse section of the fibula (at minimum circumference), a transverse section of a dorsal rib fragment, and a transverse section of a small gastralium fragment.

In the fibula (Figure S3A), very little primary tissues remains visible, and at least 3-4 generations of secondary osteons are identifiable in the inner cortex. An EFS is visible in the periosteal margin, but otherwise no growth marks are identifiable (with their record erased through tissue remodeling). The femur wedge section (Figure S3B) preserves a transect of cortex from the periosteal to endosteal margin. The inner 1/4 of the cortex is moderately remodeled, with primary tissue still visible in places but otherwise replaced with secondary osteons. In the remaining 3 /₄ of the section where primary bone tissue predominates, it is consistent with fibrolamellar bone as a woven-parallel complex. 46,47 The vascular patterns and density in the primary bone of the femur vary from laminar to plexiform arrangement over most of the cortex, particularly in the inner cortex, grading later into a mixture of plexiform to reticular in areas of the outer cortex, before reducing complexity in the outermost cortex. No inner circumferential layer is preserved. An external fundamental system (EFS; also known as an outer circumferential layer) is present in the periosteal margin, indicating skeletal maturity. The femur preserves 24 annual growth marks in the primary cortex, and an additional 4 in the EFS. At least one growth mark in the primary cortex is a 'double LAG' (i.e. 'split LAG', 'couplet', etc), and was counted as a single growth mark for aging purposes. There are additional features in the inner cortex that may represent growth marks / annuli, but which could not be determined confidently

Current Biology Report



due to the degree of remodeling. A mixture of primary and secondary tissue is observed in the sectioned dorsal rib. The rib section of MMCh-PV 65 (Figure S3C) preserves approximately 8 observable growth marks, though they cannot be effectively traced around the circumference of the section due to the combination of remodeling and extensive taphonomic alteration/staining, the latter previously referred by other authors to be the result of fungal or bacterial activity. The preserved growth marks appear to also include multiple 'double LAG' sets, though given the difficulties tracing their extent over the circumference of the cortex, it is difficult to confidently determine if these represent 'double LAGs' or closely-spaced but distinct LAGs. The sectioned gastralium (Figure S3D) preserves a similar pattern to that observed in the fibula, where secondary tissue predominates, and an EFS is observable in the periosteal margin, alongside isolated areas primary tissue.

See Cullen et al.²⁶ for additional histological descriptions, growth curves, and age retrocalculations of this specimen, alongside comparisons to other theropods. To summarize the relevant results of that study, MMCh-PV 65 was estimated as a mature individual of 39-53 years of age at death. The lack of additional individuals (particularly from earlier ontogenetic stages) limits our ability to further narrow this age range, and consequently aspects of the growth pattern, but it is nonetheless notable that this individual preserves approximately double the number of growth marks in the primary tissue of its femur when compared to the oldest known individual of *Tyrannosaurus rex* (FMNH PR 2081), despite the femur of the latter being approximately 10-20% larger than the former, and both specimens preserving a similar proportion of primary to secondary tissue in their femoral sections.²⁶ This would indicate that although the precise ontogenetic age of MMCH-PV 65 cannot yet be fully resolved, it can be said that it reached maturity at a considerably older age than did *T. rex*. Further, this range of ontogenetic age estimates would suggest MMCh-PV 65 is among the ontogenetically oldest dinosaurs currently known, and the oldest non-avian theropod known to date. Growth comparisons of this specimen to a variety of coelurosaurs, allosauroids, and other theropods suggests that *Meraxes gigas* reached 'gigantic' size through a hypermorphic modification to the allosauroid growth pattern, remaining actively growing for a longer period of time when compared to other allosauroids (e.g., *Allosaurus*) while growing at similar rates.²⁶

As a note, the estimated femoral circumferences for MMCh-PV 65 in Cullen et al.²⁶ were based on estimates made at the time the sample was obtained for sectioning. More recent re-measurements (for this study) have adjusted the estimated circumference of the right femur (at the sectioning site) to be 475 mm. While this is different from the original estimate used in the growth analyses, and the minimum femoral circumference for this specimen (452 mm, from the more complete left femur) is even smaller, this does not significantly impact the results of the interspecific growth analyses in that study as they focused on proportional annual differences in circumference rather than the absolute maximum values. Additionally, following the methods outlined in Cullen et al.,²⁶ we have re-estimated the LAG circumferences based on these revised femur circumferences, and calculated comparative growth curves and age retrocalculations (Figure S3E). Comparing these revised versions to those published in Cullen et al.²⁶ demonstrates that they do not significantly impact the growth curves and age retrocalculations presented in that study (or their related evolutionary inferences).

Technical details on the fieldwork and extraction activities

The holotype specimen of *Meraxes* comes from a lag deposit containing the partially articulated (Figures S4A and S4B) or associated remains of at least four dinosaurs including a titanosaurid represented by several articulated dorsals and two rebacchisaurid specimens. Although there was some overlap between parts of the more complete rebacchisaurid specimen and the skeleton of *Meraxes*, their remains are easily distinguishable by size and morphology. The initial discovery was made in 2012 and excavations took place over 4 seasons between 2012 and 2014. Overburden was removed using a jackhammer, rocksaw, picks and chisels (Figure S4C). Excavation of individual bones was carried out using hand tools and fossils were wrapped in plaster and bandages prior to removal (Figure S4D). Removal of the largest jackets including one containing the articulated pelvis and sacrum was done with a small custom-built buggy. During the excavation of the specimen, 15-20% Paraloid B-72 in acetone solution was used as a consolidant and viscous 'koob tubes' with 50% B-72 in acetone solution was used as a field adhesive. Five minute epoxy was also used as an adhesive for larger fragments. The same consolidants and adhesives were used in the lab while preparing the specimen. The specimens were prepared with standard manual and mechanical preparation methods using air scribes.

The partially articulated skeletons were excavated at the contact of a mudstone layer representing an overbank deposit and an overlying sandstone layer approximately 2 meters thick that represents a massive sheet flow or similar high energy flooding event. While most of the bones were excavated from the underlying mudstone, some were suspended at the bottom of the sandstone where it formed an overhang above the softer and more eroded mudstone. These bones included several fragile cranial elements.

To collect these fossils and their associated impressions exposed on the underside of the weather resistant sandstones (Figure S4E) our team applied a thin layer of silicone caulk as a separator between the fossils and plaster jacket, because the wet tissue paper would not adhere to the overhang (Figure S4E). We then applied wet plaster to the caulked area to generate adhesion for subsequent application of plaster bandages, which would otherwise want to unwrap from the rock surface due to gravity.

A liberal application of consolidants and mold releasing agent prior to application of the silicone caulk resulted in superb preservation of the fossil bones and impressions and in excellent separation between the specimen and matrix and the silicone caulk during preparation. The use of silicone caulk as a separator was also found to be effective for a specimen left *in situ* for future excavation, because the silicone caulk created an anoxic environment, which is more resistant to weathering and erosion.





Nomenclatural acts

The nomenclatural acts performed in this work have been registered in ZooBank. The Life Science Identifiers (LSDI) for this publication are: urn:lsid:zoobank.org:pub:CE29E6EB-DC13-4563-9CCA-CD176A82BF78.

QUANTIFICATION AND STATISTICAL ANALYSIS

Body mass estimation

The body mass of the holotype specimen of *Meraxes gigas* (MMCh-PV 65) was estimated through the equation for non-avian biped dinosaurs presented by Campione and colleagues, ⁵¹ which is:

$$log_{10} BM = 2.754.log_{10} (CF) - 0.683.$$

where BM is the body mass and CF is the minimum femoral circumference of the femur, which in the this case is 452 millimeters. The specific calculation was performed using the associated MASSTIMATE package in R,⁵² giving a result of 4263 kg (confidence interval of 3196 kg - 5331 kg) (see Figure S3).

Analysis on skull dimensions in Giganotosaurus

Meraxes skull only lacks the premaxillae and minor palatal elements, like the vomer. The premaxilla length was scaled from that of Giganotosaurus plus the orientation and the continuation of the curvature of the the anterior border of the premaxillary process of both nasals. This makes the anteroposterior length estimate for Meraxes' skull very precise. To estimate skull length in Giganotosaurus (from the anterior end of premaxilla to posterior end of quadratojugal), using the almost complete skull of Meraxes gigas, several measurements were taken on cranial remains of both holotypes.

Every measurement was made on homologous, undistorted and complete parts of selected bones (Data S2). They were taken with a digital caliper, or in cases exceeding 150 mm, with a regular measuring tape. Linear regressions between both skulls considering anteroposterior, dorsoventral and lateromedial and total morphological data, analyzed with Excel 2016 statistics tools, shows a good correlation for each set of measurements. All statistical information of the variable correlations are summarized in Data S2. The anteroposterior correlation slope value is 1.223 with a R² of 0.9704 (N=5; Confidence interval of slope at 95 %: 0.830/1.616). The dorsoventral correlation slope value is 1.279 and R² is 0.9992 (N=7; Confidence interval of slope at 95 %: 1.236/1.327) The lateromedial correlation slope value is 1.284 and R² is 0.9517 (N=9; Confidence interval of slope at 95 %: 1.025/1.542). This indicates that *Meraxes* skull is proportionally narrower compared with *Giganotosaurus*, nevertheless anteroposterior measurements can be considered as reliable for comparisons given that the general correlation of both cranial measurements sets shows a very good fit (R² = 0.9949) with a correlation slope value of 1.268 (N=21; Confidence interval of slope at 95 %: 1.224/1.311). Applying this value as a scaling factor yields an estimate for *Giganotosaurus*' skull length of 163.4 cm, with a confidence interval between 157.8 and 168.8 cm, at a 95 % probability.

There are several theropod species with skulls that would have surpassed 1 meter in length, but few of them are complete, and most have length estimates based on disarticulated elements. Apart from *Meraxes* (127cm) and *Acrocanthosaurus* (123 cm), other giant theropods with complete skulls are *Deinocheirus mirificus*, with a length of 102 cm,⁵³ and "Sue" specimen of *Tyrannosaurus rex*, with a length of 140 cm.⁵⁴

With respect to incomplete specimens with approximate length estimates: the neotype of the carcharodontosaurid *Carcharodontosaurus saharicus*, represented by a partial skull is estimated to be between 142 cm, ⁵⁵ to 160 cm. ⁷ The megalosaurid *Torvosaurus gurneyi* has an estimated skull length of 115 cm, based on an isolated maxilla. ⁵⁶ The largest reported theropod skull corresponds to a specimen assigned to *Spinosaurus* sp. with an estimated length of 175 cm, ⁵⁷ but given recent reconstructions based on this material, that measurement may be overestimated. ⁵⁸ With a new and reliable estimate of about 163.4 cm, *Giganotosaurus* skull is still one of the largest theropod skulls ever recorded.

Convergence analysis

We measured convergence by comparing how morphological similarity changed between ancestors and descendants using four metrics. We estimated branch-lengths by applying the cal3 method, 59 to a composite phylogeny of theropods with lambda=0.1, mu=0.08, and psi=0.1. Given the uncertainty in time-scaling, we re-scaled the tree 100 times and recalculated the convergence metrics for each rescaled tree. The degree of convergence was determined by comparing the observed difference between tips and their estimated ancestors to the differences seen in 1000 randomly evolving traits along each of the 100 time-scaled trees. Proportional (C1), absolute (C2), and lineage-scaled (C3) convergence for the three clades were determined by determing what proportion of the 100 simulated Brownian traits showed less extreme values for each of the four convergence metrics than the empirical data following the procedure laid out in Stayton. We repeated this randomization-comparison for each of the 100 time-scaled trees to produce a distribution of 100 p-values for each convergence metric that incorporated the uncertainty in the branch lengths of the empirical trees (Figure 3A). Similar results were found using Ridge Regression. Our analyses of convergence in theropod limb ratios were based on the dataset of Benson and Choiniere, as updated by Apesteguía et al. Data for a handful of taxa and specimens described in the interim, such as Deinocheirus (47) were added, as were the measurements for Meraxes. All data were log-transformed prior to analyses. The composite theropod phylogeny used to perform a phylogenetic PCA by Apesteguía et al. Were adding branches for Meraxes, and other newly included taxa, and was calibrated using stage-level temporal

Current Biology Report



information Each of the 100 trees was also used for the convergence analyses for the phylogenetically informed PCA (S15) shown in Figure 3B. Simulation means and standard deviations for each metric and combination of taxa used in the analysis can be found in Data S3 file. Data including tree files, taxon ages and measurements, and R code to perform analyses are available at: https://github. com/paleomitchelljs/Carcharodontosaur.

As was stated in the main text of this study, we propose that a lower bound, or constraint, exists around a forelimb/femur ratio of 0.4 to explain how carcharodontosaurids, abelisaurids and tyrannosaurids arrive at remarkably similar degrees of arm reduction despite the variance within each lineage. We hypothesize that this lower bound is related to the development of the pectoral girdle. Even though the forelimb is reduced in these three lineages, their scapulo-coracoids are not, and would have served as origins for relatively large muscles that insert on the humerus as reconstructed by Lipkin and Carpenter³³ for Tyrannosaurus and by Burch for Majungasaurus. 28 Fitting insertion points for muscles such as the M. coracobrachialis, M supracrocoideus, and M. pectoralis would likely set a constraint on how small the humerus, and consequently the limb as a whole, can get. In birds that lose part, or all, of the forelimbs, the pectoral girdle is either heavily reduced (hesperornithiforms) or completely lost (moas), lending some support to this hypothesis.

We further tested this constraint by examining how skull size scaled with arm reduction using a phylogenetic regression. We modeled total arm length as a function of femur length, interguadrate (IQ) width, and the interaction between femur and IQ width while accounting for the covariance structure of the tree by assuming a Brownian Motion model of trait change. 40 We used interquadrate width as our estimate of skull size as it is commonly used in herpetological literature for comparing taxa with very different snout lengths, and abelisauroids have substantially shorter snouts than tyrannosauroids or carcharodontosauroids. All data were meancentered and scaled by standard deviation to put them in identical units and aid in estimation. Unfortunately, few taxa have complete femora, arms, and an estimate of skull width, limiting our sample size to only 23 taxa. Femur length, interquadrate width, and the interaction of the two were used to predict arm length in those 23 theropod taxa using the R package "phylolm" assuming a Pagel's lambda model of trait evolution (Table S4). The multiple regressions find statistically clear effects for femur length on arm length (slope = 1.08 ± 0.12) but not for skull width (-0.01 ± 0.12). The interaction term is estimated to be negative (-0.13 ± 0.07), which says that as skull size increases, the relationship between femur length and arm length decreases.